PERGAMON

International Journal of Multiphase Flow 26 (2000) 1545–1564

International Journal of Multiphase Flow

www.elsevier.com/locate/ijmulflow

A model for red blood cell motion in bifurcating microvessels

A.W. El-Kareh*, T.W. Secomb

Department of Physiology, University of Arizona, Tucson, AZ 85724-5051, USA

Received 29 April 1998; received in revised form 17 August 1999

Abstract

A theoretical model is developed for red blood cell motion in a diverging microvessel bifurcation, where the downstream branches are equal in size but receive different flows. The model is used to study migration of red cells across streamlines of the underlying flow, due to particle shape and flow asymmetry. Effects of cell–cell interactions are neglected. Shapes of flowing red cells are approximated by rigid spherical caps. In uniform shear flows, such particles rotate periodically and oscillate about fluid streamlines with no net migration. However, net migration can occur in non-uniform flows due to the particles' lack of fore-aft symmetry. A nonuniform flow field representative of a bifurcation is developed: flow bounded by two parallel plates, and divided by a cylindrical post. Significant migration is found to occur only with a nonuniform and asymmetric distribution of upstream orientations. The model suggests that the assumption made in previous models of bifurcations, that red cells follow fluid streamlines, is justified if cells approach the bifurcations with random orientations.

Keywords: Bifurcation; Blood; Microcirculation; Spherical cap; Phase separation; Migration; Stokes flow; Red cell

1. Introduction

When blood flows through a diverging bifurcation in a microvessel, the hematocrits (volume fractions of red blood cells) in the two downstream branches are generally unequal. This "phase separation" leads to an uneven distribution of hematocrit in the vessels of the

* Corresponding author.

0301-9322/00/$ - see front matter
PII: S0301-9322(99)00096-8

microcirculation, which significantly influences its oxygen-carrying characteristics. Experimental observations (Pries et al., 1989) show that, if the two downstream branches are similar in size, the branch with the higher flow rate generally receives a higher hematocrit than the other branch. Details of the bifurcation geometry, such as the angles between the upstream and downstream vessels, have little effect on this behavior. However, the distribution of hematocrit is dependent on the diameters of the vessels and the hematocrit in the parent vessel.

Unequal hematocrit distribution can result from two main factors: non-uniform red cell distribution in the upstream vessel, and deviation of red cell trajectories from fluid streamlines in the vicinity of the bifurcation. Most previous theoretical analyses of this phenomenon (Schmid-Schönbein et al., 1980; Perkkiö and Keskinen, 1983; Fenton et al., 1985; Rong and Carr, 1990; Enden and Popel, 1992) have focused on the effects of non-uniform upstream red cell distribution, assuming that red cells follow fluid streamlines. The concentration in each downstream vessel is then determined by the concentration in the region of the upstream vessel that feeds it (its upstream "fluid capture tube"). Hematocrit is generally low in a region near the wall of the upstream vessel (the "plasma layer"). The fluid capture tube of the branch with lower flow includes proportionally more of this region, and so, that branch receives a lower hematocrit than the other branch. This effect is known as "plasma skimming".

The assumption that red cells follow the streamlines of the flow in the absence of cells is reasonable for vessels with diameters much larger than a single cell. However, phase separation is stronger in smaller bifurcations, where this assumption is less justifiable. If the cell is not small relative to the characteristic dimensions of the flow field in the bifurcation, its center of mass may deviate significantly from the fluid streamlines of the basic flow. This is known as "red cell screening" (Pries et al., 1981) because it results from the finite size of red cells relative to the diameters of the vessels that they are entering. Such migration across streamlines, which may contribute to the unequal hematocrit distribution in bifurcations, is considered in this study. The Reynolds number is much less than one and Stokes flow is assumed. Effects of interactions between particles are neglected. The hematocrit (volume fraction of red blood cells) in bulk human blood is typically in the range 40–45%, but a wide range of hematocrits, including very low values, is observed in microvessels, as a result of phase separation. Results for low hematocrits are therefore physiologically relevant. Experimental data of Ditchfield and Olbricht (1996) for rigid spheres, and Pries et al. (1989) for red cells in vivo suggest that phase separation is actually strongest at very low hematocrits. At higher hematocrits, multi-particle interactions may influence phase separation, but such effects are not considered here.

The motion of a suspended (neutrally buoyant) particle in a fluid depends both on its shape and on the flow field. The effect of the flow field may be seen by considering a local Taylor expansion of the velocity field about the particle center. In a linear flow, the center of a sphere must follow a fluid streamline. However, non-spherical particles may deviate from streamlines. The term "shape-dependent migration" is used here for deviation from streamlines, under conditions where spherical particles would not deviate.

If the second derivatives of the flow field are nonzero (or equivalently, the pressure gradient is nonzero), a spherical particle can deviate from streamlines. According to Faxen's Law (Happel and Brenner, 1973), the particle's velocity relative to the base flow at its center is $a^2\nabla p/(6\eta)$, where p is the hydrodynamic pressure, a is the radius, and η is the fluid viscosity. While this result is exact only for an unbounded fluid, it is a good approximation for bounded

flows provided that the particle is not too close to the boundaries. Since this effect results in migration in the direction of increasing pressure, it is referred to as "pressure-gradient migration."

Yan et al. (1991) and Wu et al. (1992) studied the trajectories of spherical particles near a circular hole in a plane boundary with a shear flow over it, as a model for flow in a bifurcation with a side branch which is much smaller than the parent vessel. The reduction of particle concentration due to the plasma skimming effect in such a bifurcation was analyzed by Yan et al. (1991). Interactions between finite-sized particles and the walls were considered by Wu et al. (1992) who showed that the concentration in the side branch could be further reduced by "screening" effects. The suction applied to the side branch results in particle migration away from the branch, in accordance with Faxen's Law.

The aim of the present study is to analyze the trajectories of particles approaching the dividing surface in a bifurcation whose downstream branches have approximately equal diameters. In the microcirculation, such bifurcations occur more frequently than bifurcations with one side branch that is much smaller than the parent vessel. The dividing surface (the part of the wall lying between the downstream vessels) is generally curved, not sharp-edged as assumed by Yan et al. (1991) and Wu et al. (1992). Particle migration across streamlines contributes to unequal hematocrit distribution when it causes particles to cross the separating streamsurface, i.e., the surface separating the upstream "capture tubes" of the two downstream vessels. Therefore, the emphasis here is on the motion of particles approaching the flow divider, whose trajectories lie near the separating streamsurface. Such particles typically originate in the central part of the flow of the parent vessel, and their interactions with the dividing surface are likely to be more important than their interactions with other parts of the vessel walls in determining which branch they enter.

Based on these considerations, the following configuration is assumed. The dividing surface is represented by a cylindrical post of finite height, whose curvature corresponds to the curvature of the dividing surface. The domain is bounded above and below by parallel plates. This allows imposition of an overall pressure gradient to drive the flow, which is not possible if the domain is infinite in three dimensions. The distance between the plates corresponds to the diameter of the downstream vessels. This geometry has the advantage that the basic flow in it can be calculated analytically, but it retains important features of the actual bifurcation. Unequal flows in the downstream vessels are represented by asymmetry of the flow impinging on the post.

Red cells are not generally spherical and often have asymmetric shapes; this may influence their trajectories. Both spherical and non-spherical particles are considered here. Particle motions are computed from local linear and quadratic approximations to the basic flow in the vicinity of the particle. This approach is appropriate for vessels with diameters several times that of a red cell, in which cells are not in close proximity to vessel walls. It neglects the effect of flow field boundaries on the perturbation of the flow field by the particle, and its validity is therefore limited when particles are very close to the flow divider.

Although red cells are highly deformable, their membranes possess significant viscous resistance to shear deformation. Typically, red cells traverse bifurcations in a short time (of the order of milliseconds) and their shape change during this period is likely to be slight. Therefore, in this analysis, fixed particle shapes are assumed. For studying shape-dependent

migration, orthotropic particles (particles with three orthogonal planes of symmetry) cannot be used. This includes spheres, disks, ellipsoids, and biconcave disks, all of which follow fluid streamlines in a shear flow (Bretherton, 1962). Several experimental studies have used such shapes (Ditchfield and Olbricht, 1996; Chien et al., 1985; Bugliarello and Hsiao, 1964), and therefore could not include shape-dependent migration. A simple shape that will migrate off fluid streamlines in a shear flow is the (hollow) spherical cap. The spherical cap shape is suggestive of experimentally observed red cell shapes, not only in narrow tubes, but also in larger tubes where red cells exhibit multifile flow (Skalak and Branemark, 1969; Goldsmith and Karino, 1980). Red cells were modeled as rigid spherical caps in the experimental study of Hochmuth and Sutera, 1970. The theoretical model of Barnard et al. (1968) for red cell motion in tubes led to parachute-shaped cells resembling spherical caps. From these considerations, the spherical cap was chosen to study shape-dependent migration here.

2. Formulation of the model

The model used to study particle migration is now formulated. First, the asymmetric divided flow that is used to study both shape-dependent migration and pressure-gradient migration is developed. This is done in two steps: in Section 2.1.1, a suitable asymmetric flow in the absence of the dividing surface (cylindrical post) is determined. Asymmetrically divided flow in a bifurcation with symmetric geometry can be represented as the superposition of a flow divided symmetrically between the two downstream branches, and a flow from the low-flow branch into the high-flow branch, with no net flow in the parent vessel (Fig. 1a). Plane Poiseuille flow is an obvious choice for the symmetric component. An asymmetric flow with the desired behavior upstream of the bifurcation that has a simple analytical expression is chosen. Then in Section 2.1.2, the disturbance flow due to the post is computed, with the particles still absent. Behavior of the flow downstream of the bifurcation has no effect on distribution of particles and is therefore ignored here. In Section 2.2, the equations for shape-dependent migration of the model particles (spherical caps) in the flow are presented. For pressure-gradient migration, the Faxen's Law approximation is used; this simple equation does not require a separate section for its presentation.

2.1. Fluid flow in a model bifurcation

A Cartesian coordinate system (x, y, z), and a cylindrical coordinate system (r, θ, z) are used, as shown in Fig. 1a. They are related by $x = r\cos\theta$, $y = r\sin\theta$, with the z-axis the same for both. The parallel plates are located at $z = -h$ and $z = h$. The cylindrical post is described by $r = R$, for $-h \le z \le h$. The main direction of flow is the x-direction. It is convenient to decompose it into two components: the flow $(\mathbf{u}, p)$ between parallel plates in the absence of the post; and the disturbance flow $(\mathbf{v}, q)$ caused by the presence of the post.

2.1.1. Flow in the absence of the cylindrical post

The two components, symmetric and asymmetric, are represented in the model system by flows $\mathbf{u}_s$ and $\mathbf{u}_a$, respectively. The symmetric part is chosen as uniform plane Poiseuille flow, the

two-dimensional analog to Poiseuille flow in a cylindrical tube:

$$\mathbf{u}_s = \mathbf{e}_x A\left(1 - \frac{z^2}{h^2}\right), \tag{1}$$

where A is a constant. Near the dividing surface, the asymmetric flow is approximately in the sideways $(-y)$ direction. (In what follows, the high flow side will be to the right when facing the dividing surface from upstream.) For simplicity, a unidirectional flow $\mathbf{u}_a = \mathbf{e}_y u_y(x, z)$ is therefore chosen. Then the pressure gradient $\mathrm{d}p/\mathrm{d}y$ must be a constant. The asymmetric flow should approach zero in the upstream $(-x)$ direction, and must satisfy no-slip at the two plane walls $z = \pm h$. This implies that $\mathrm{d}p/\mathrm{d}y = 0$, so u_y satisfies:

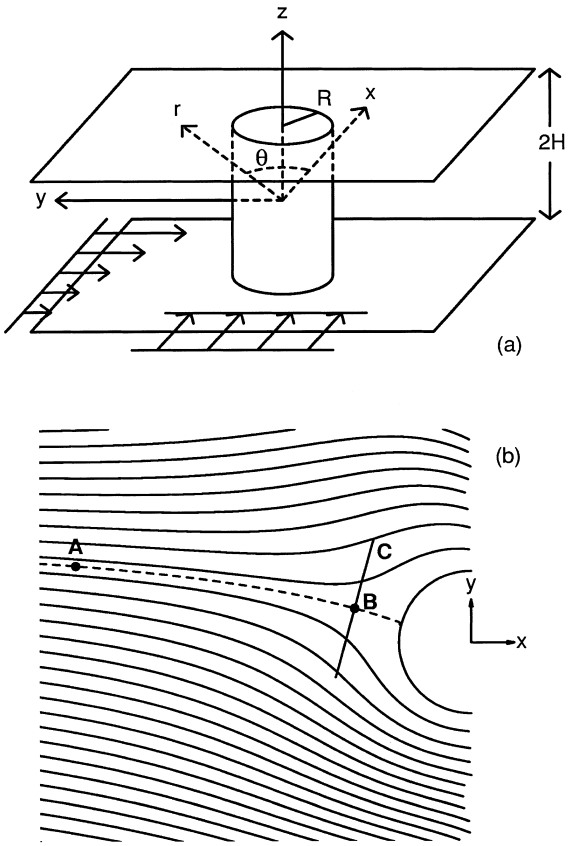

Fig. 1. (a) The geometry of the cylindrical post between two parallel plates, showing the Cartesian and cylindrical coordinate systems used in computing the flow. The two components of the flow (undisturbed by the post) are shown: symmetric (plane Poiseuille flow in x direction) and asymmetric flow in y direction (decaying exponentially upstream). (b) Streamlines of the base flow in the model bifurcation, for $B/A = 1$, $R = 0.5$ and $h = 1$. Fluid separating streamline is shown dashed. Dot (A) shows starting point for particle trajectories. Dot (B) is the chosen reference point on the separating streamline. Reference line (C) is used in Fig. 7 to evaluate particle orientation change and migration.

$$\frac{\partial u_y^2}{\partial x^2} + \frac{\partial u_y^2}{\partial z^2} = 0, \tag{2}$$

with possible solutions of the form:

$$u_y = \cos\left(\frac{n\pi z}{2h}\right) \exp\left(\frac{n\pi x}{2h}\right), \tag{3}$$

where n is an odd positive number. This solution decays exponentially upstream from the dividing surface, which is the expected decay for the disturbance due to an obstacle in a bounded flow. Downstream it grows unboundedly; however, only the motion in the upstream region is considered here. The case $n = 1$ corresponds to a flow profile with no reversals, and is assumed here. The overall flow in the absence of the post is therefore:

$$\mathbf{u} = \mathbf{e}_x A\left(1 - \frac{z^2}{h^2}\right) - \mathbf{e}_y B \cos\left(\frac{\pi z}{2h}\right) \exp\left(\frac{\pi x}{2h}\right), \tag{4}$$

where B/A measures the extent to which the flow is asymmetric.

2.1.2. Disturbance flow caused by cylindrical post

A flow $\mathbf{v}$ must now be calculated to cancel $\mathbf{u}$ on the cylindrical post, while satisfying no-slip at the plane walls and decaying with distance from the post. Lee and Fung (1969) developed a solution for such a flow when the base flow is plane Poiseuille, which can be extended for the present case. Their solution in cylindrical coordinates has the general form:

$$v_r = \frac{\partial \phi_0}{\partial r}\left(1 - \frac{z^2}{h^2}\right) - Re\left[\sum_{n=1}^{\infty} \frac{1}{\alpha_n^2} \frac{\partial \phi_n}{\partial r} \frac{\mathrm{d}q_n}{\mathrm{d}z}\right] - \sum_{n=0}^{\infty} \frac{1}{r} \frac{\partial \psi_n}{\partial \theta} \cos(k_n z); \tag{5}$$

$$v_\theta = \frac{1}{r}\frac{\partial \phi_0}{\partial \theta}\left(1 - \frac{z^2}{h^2}\right) - Re\left[\sum_{n=1}^{\infty} \frac{1}{\alpha_n^2 r} \frac{\partial \phi_n}{\partial \theta} \frac{\mathrm{d}q_n}{\mathrm{d}z}\right] + \sum_{n=0}^{\infty} \frac{\partial \psi_n}{\partial r} \cos(k_n z); \tag{6}$$

$$v_z = Re\left[\sum_{n=1}^{\infty} \phi_n q_n\right]; \tag{7}$$

and the pressure is

$$p = -\frac{2\eta}{h}\left\{\frac{\phi_0}{h} + Re\left[\sum_{n=1}^{\infty} \phi_n \frac{\cos(\alpha_n z)}{\cos(\alpha_n h)}\right]\right\}. \tag{8}$$

In this solution, the functions $\phi_n(r, \theta)$ and $\psi_n(r, \theta)$ are any solutions of

$$\nabla^2 \phi_n - \alpha_n^2 \phi_n = 0 \tag{9}$$

and

$$\nabla^2\psi_n - k_n^2\psi_n = 0, \tag{10}$$

respectively, where $k_n = (2n+1)\pi/(2h)$. The functions q_n are defined by

$$q_n(z) = \frac{\sin \alpha_n z}{\sin \alpha_n h} - \frac{z \cos \alpha_n z}{h \cos \alpha_n h}, \tag{11}$$

with the complex eigenvalues α_n, $n = 1, 2, 3, \ldots$, chosen to satisfy $\sin 2\alpha_n h = 2\alpha_n h$.

Now, the velocity field (4) at the post surface, when expressed in cylindrical coordinates and expanded in Fourier series, yields:

$$u_r|_{r=R} = \sum_{n=1}^{\infty} a_n \cos(k_n z) \cos\theta + \sum_{m=1}^{\infty} b_m \cos(k_0 z) \sin m\theta; \tag{12}$$

$$u_\theta|_{r=R} = \sum_{n=1}^{\infty} c_n \cos(k_n z) \sin\theta + \sum_{m=0}^{\infty} \mathrm{d}_m \cos(k_0 z) \cos m\theta; \tag{13}$$

(with $u_z = 0$), where the Fourier coefficients are

$$a_n = -c_n = \frac{32A(-1)^n}{\pi^3(2n+1)^3}; \tag{14}$$

$$b_m = -B\big(I_{m-1}(k_0 R) - I_{m+1}(k_0 R)\big); \tag{15}$$

$$d_m = \begin{cases} -BI_1(k_0 R) & m = 0; \\ -B\big[I_{m-1}(k_0 R) + I_{m+1}(k_0 R)\big] & m > 0; \end{cases} \tag{16}$$

and where the I_m are Bessel functions of the second kind.

The form of these expansions suggests the following choices for ϕ_n and ψ_n:

$$\phi_0(r, \theta) = \frac{A_0'}{r}\cos\theta + \sum_{m=1}^{\infty} A_{0,\,m}\frac{1}{mr^m}\sin m\theta; \tag{17}$$

and for $n > 0$

$$\phi_n(r, \theta) = \big(A_n' + iB_n'\big)K_1(\alpha_n r)\cos\theta + \sum_{m=1}^{\infty}\big(A_{n,\,m} + iB_{n,\,m}\big)K_m(\alpha_n r)\sin m\theta; \tag{18}$$

and for $n \geq 0$

$$\psi_n(r, \theta) = C_n' K_1(k_n r)\sin\theta + \sum_{m=0}^{\infty} C_{n,\,m} K_m(k_n r)\cos m\theta; \tag{19}$$

where $A_{n,\,m}$, $B_{n,\,m}$, $C_{n,\,m}$, A_n', B_n' and C_n' are arbitrary (real-valued) constants. The functions K_m appearing in these expressions are MacDonald's functions (modified Bessel functions of the

third kind), which decay with r for $m \geq 0$. The corresponding expressions of Lee and Fung (1969) involve only the $m = 1$ terms, because of the symmetry of their base flow (plane Poiseuille flow). Here, the addition of a decaying transverse flow makes it necessary to add a series of harmonics in θ. A similar extension to higher harmonics was made by Tsay and Weinbaum (1991) in their analysis of multiple cylindrical posts (in a square periodic array) between two plates.

This general solution identically satisfies the no-slip conditions on the plane boundaries. It remains to evaluate the unknown coefficients so as to satisfy the boundary conditions on the post. The details of this procedure are given in Appendix A. The general approach is to expand the components of **u** and **v** at the post in terms of suitable orthonormal bases and to equate the coefficients to zero. For the r and θ components, a double Fourier series in θ and z is used. However, the z component of velocity is odd in z, and a trigonometric Fourier expansion in z would yield terms that do not satisfy the boundary conditions at $z = \pm h$. An alternative set of basis functions $Y_n(z)$ is therefore used (Lee and Fung, 1969). The resulting set of linear equations for the coefficients is truncated at $n = 4$ and $m = 4$ and solved numerically. Fig. 1b shows streamlines of the flow in the plane midway between the two plates. In all computations (Figs. 1b and 4–7), the plate spacing is chosen as $h = 1$ and the post radius is $R = 0.5$. The numerical solutions for **u** and **v** cancel each other to within 0.1%, and the velocities on the plates are $O(10^{-6})$, compared with $O(1)$ velocities near the midplane, indicating that the error in satisfying the no-slip conditions on the post and plates is very small.

Once the undisturbed fluid flow has been determined, the fluid dividing streamline can be determined. The parameter B/A can be interpreted as giving a flow fraction, by assuming that the distance between the two parallel plates represents the upstream tube diameter. The flow in the vessel is then interpreted as the flow between the streamlines at $y = -h$ and $y = h$ far upstream. Then for the above values of h and R, for $B/A = 0$ the flow fraction in the high flow downstream vessel is 0.5, for $B/A = 0.5$ it is 0.72, and for $B/A = 1.0$ (as in Fig. 1b) it is 0.93. (These flow fractions are based on flow in the midplane $z = 0$; from experimental results of Rong and Carr (1990) for the shape of the entire dividing streamsurface, the flow fraction in the midplane is close to the flow fraction for the entire tube.)

2.2. Motion of spherical caps in a flow field

The equations for the motion of spherical caps in a flow field are now developed. The particle motion is approximated at any instant in time using the local linear component of the flow, as if that flow was uniform and unbounded. As the particle changes position, however, this local linear component varies. Mathematically, this corresponds to using the first term in a Taylor series expansion of the flow about the chosen particle reference point, and using only the first "reflection" in a method of reflections expansion (Happel and Brenner, 1973). It will be shown below that migration due to the quadratic variation of the flow is relatively much smaller. Therefore, in the following subsection, the equations governing the motion of the model asymmetric particles (spherical caps) in linear flow fields are presented.

The motion of a spherical cap in a linear flow field may be determined from the complete resistance tensor, which was computed in a series of papers summarized by Dorrepaal (1984).

For a neutrally buoyant body of revolution, the particle velocity U_i in a linear flow w_i with a rate-of-strain tensor e_{ij} and vorticity $2\omega_i$ is (Nir et al., 1975):

$$U_i = w_i + \left[\gamma\left(\frac{1}{2}\delta_{ik}p_l + \frac{1}{2}\delta_{il}p_k - p_ip_kp_l\right) + \beta\left(p_ip_kp_l - \frac{1}{3}p_i\delta_{kl}\right)\right]e_{kl}. \tag{20}$$

Here, Cartesian coordinates (X_1, X_2, X_3) are used. The unit vector p_i points along the particle axis and gives its orientation. The motion of this vector is given by (Nir et al., 1975)

$$\frac{\mathrm{d}p_i}{\mathrm{d}t} = b(e_{ik}p_k - e_{kl}p_lp_i) + \epsilon_{ijk}\omega_jp_k. \tag{21}$$

In these equations, the particle is described by three constants, γ, β and b, which are related to the resistance tensor as follows:

$$\gamma = 2\frac{b_1q_1 - d_1r_1}{a_1b_1 - d_1^2}; \tag{22}$$

$$\beta = \frac{q_3}{a_3}; \tag{23}$$

and

$$b = 2\frac{a_1r_1 - d_1q_1}{a_1b_1 - d_1^2}. \tag{24}$$

(A sign error in the expression for γ as given by Nir et al. (1975) has been corrected here.) The constants a_1, a_3, b_1, d_1, r_1, q_1 and q_3 appear in the resistance tensor of the particle (Nir et al., 1975), and they depend only on the cap angle α and radius a, and the point chosen as the origin. It is convenient to take the origin to be the center of reaction. This is defined by Happel and Brenner (1973) for any rigid particle as the unique geometrical point with reference to which the coupling tensor in the full hydrodynamic resistance tensor is symmetric. Kim and Karrila (1991) use the term "center of hydrodynamic resistance" for this point.) From the standpoint of hydrodynamic behavior, this point is more meaningful than the center of mass (for a spherical cap, unlike for orthotropic particles, these two centers do not coincide). Formulas for the values of the constants a_1, etc., are given by Dorrepaal (1984) and he also tabulates their values for this choice of origin. Fig. 2 shows the variation of the parameters β, γ and b with cap angle α. While b is independent of cap radius a, both β and γ are proportional to a. In Fig. 2, a is chosen for each cap angle to give all caps the same area 0.46 (that of a cap with $a = 0.5$, $\alpha = \pi/4$). The area is held fixed to correspond to red cells, which have nearly constant area.

Fig. 3 shows the trajectory of the center of reaction of a cap in a simple shear flow $u_1 = X_2$, starting at the origin. The center of reaction makes a significant excursion, mainly in the X_1 direction, returning to its original position after one complete revolution of the particle. In contrast, the center of reaction of an orthotropic particle placed in this flow remains at the

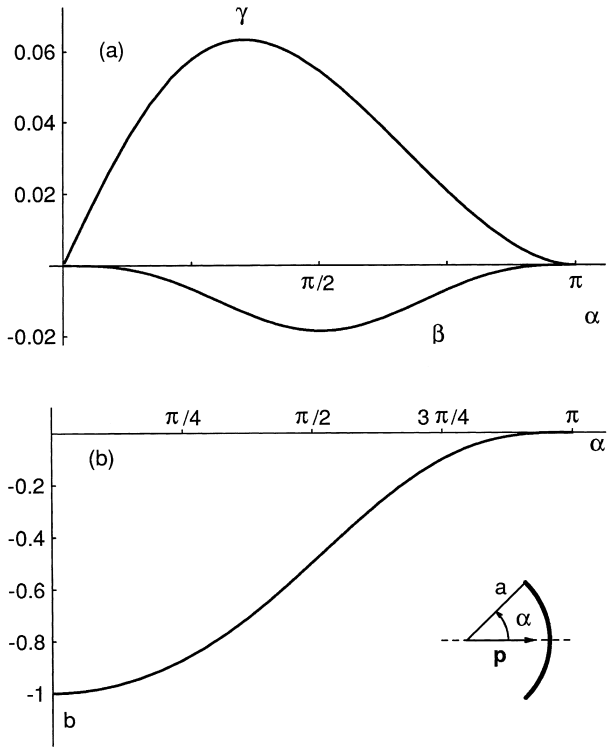

Fig. 2. Variation of spherical cap hydrodynamic parameters γ, β and b with cap angle α. Radius a is chosen for each α so that all caps have the same area 0.46 as a cap with $a = 0.5$, $\alpha = \pi/4$. The inset shows the definitions of cap radius a, angle α, and (unit) orientation vector **p**.

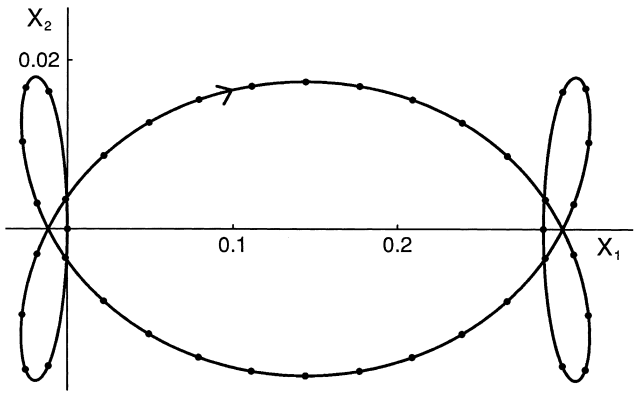

Fig. 3. Trajectory of the center of reaction of a spherical cap ($\alpha = \pi/4$, $a = 0.5$) in a simple shear flow, starting at (0, 0) on the line of zero velocity (X_1-axis) with initial orientation vector (−1, 0). Dots show positions at evenly spaced time intervals.

origin. The spherical cap's lack of fore-aft symmetry leads to instantaneous migration, although no net migration occurs over one period of the motion (cf. Bretherton, 1962).

For an orthotropic particle, the trajectory of the particle is defined by the motion of its center of reaction, which coincides with its geometric center. For a spherical cap, however, the choice of a point (fixed with respect to the cap) to define the trajectory is, to some extent, arbitrary. For almost all points, trajectories analogous to Fig. 3 show larger maximum excursion in the X_2 direction (the direction orthogonal to the fluid streamlines). Those points with smaller maximum X_2 excursions lie extremely close to the center of reaction, and have trajectories that are quite similar. Therefore, the center of reaction is a suitable reference point for defining trajectories, since it does not exaggerate the departure of trajectories from streamlines during particle rotation.

To compute trajectories, the velocity gradients appearing in Eqs. (20) and (21) are determined from a Taylor series expansion about the center of reaction, of the flow defined in Section 2.1.

For pressure-gradient migration of spherical particles, the motion is approximated by Faxen's Law:

$$\mathbf{U} - \mathbf{u}_0 = \frac{a^2}{6\eta}(\nabla p)_0, \tag{25}$$

where the subscript 0 denotes evaluation at the particle center. The left-hand side of Eq. (25) gives the deviation of particle velocity $\mathbf{U}$ from fluid velocity $\mathbf{u}$. The velocity $\mathbf{u}$ and pressure p are for the flow in the absence of the particle. Results for particle trajectories are now presented in the following section.

3. Results and discussion

In the absence of particles, a separating streamsurface extends upstream from the flow divider in a bifurcation, such that all the fluid lying on one side of this surface ultimately enters one branch. Particle migration across this surface alters the relative concentrations in the downstream branches. Such migration depends on the component of particle velocity perpendicular to the streamsurface, evaluated on it. For simplicity, we restrict attention to trajectories on the midplane ($z = 0$) of the bifurcation.

3.1. Pressure-gradient migration in the model bifurcation

As stated earlier, the velocity of the center of a sphere relative to the undisturbed flow at that point is proportional to the pressure gradient, by Faxen's Law. Migration across a streamline therefore depends on the component of pressure gradient acting normal to it. In each downstream branch of the bifurcation, the pressure decreases. This implies the existence of a point of maximum pressure on the dividing surface. The direction of particle migration can be predicted by considering the position of this maximum relative to the intersection of the separating streamline with the dividing surface. As shown in Fig. 4, the separating streamline

in an asymmetric flow lies on the low-flow side of the point of maximum pressure. The pressure gradient on the separating streamline is therefore directed towards the high-flow side near the flow divider, causing the particle migration towards the high-flow side.

The magnitude of this effect can be estimated by evaluating the pressure gradient on the separating streamline at a distance of one radius R away from the dividing surface. Using Faxen's Law, the resulting velocity correction is less than 1% of the fluid velocity. Trajectories computed with the correction are almost indistinguishable from fluid streamlines in the region up to the point where the sphere is so close to the post that the approximation cannot be used.

The study of Wu et al. (1992) for migration of spherical particles in a divided flow found a significant phase separation effect. The difference between their results and ours has two probable causes. Firstly, their computations included near-field interactions. Secondly, their assumed geometry of a circular hole in a plane leads to a flow field around a sharp-edged corner, in whose vicinity very large pressure gradients occur. In contrast, the curved flow divider used here leads to a smoothly varying pressure field. Audet and Olbricht (1987) and Amini and Fallahyan (1997) used numerical methods to predict the two-dimensional analog of pressure-gradient migration, for circular cylinders in two-dimensional bifurcating channels. Because of the significant differences between two- and three-dimensional flows, it is difficult to compare their results with the model presented here.

For non-spherical particles, the magnitude of the pressure-gradient migration, which depends primarily on particle size, is likely to be of similar magnitude to that estimated for spheres. This type of migration, which depends on quadratic variations in the flow field, appears to be a weak effect. Shape-dependent migration, discussed next, may therefore be dominant for non-spherical particles.

3.2. Shape-dependent migration in the model bifurcation

Using the equations from Section 2.2, the velocities of spherical caps in the bifurcated flow of Section 2.1 are obtained. Fig. 5 shows the migration velocity (perpendicular to the fluid

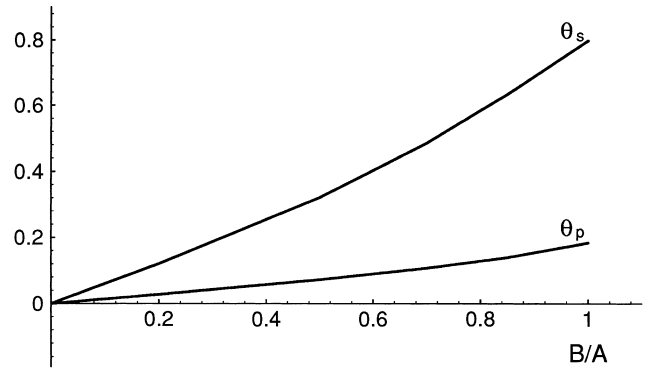

Fig. 4. The angular location on the post (in the midplane between the two plates) of the stagnation line (θ_s) and pressure maximum (θ_p), as a function of flow asymmetry B/A, for $R = 0.5$ and $h = 1$. Angles are measured in radians relative to the stagnation point for symmetric flow.

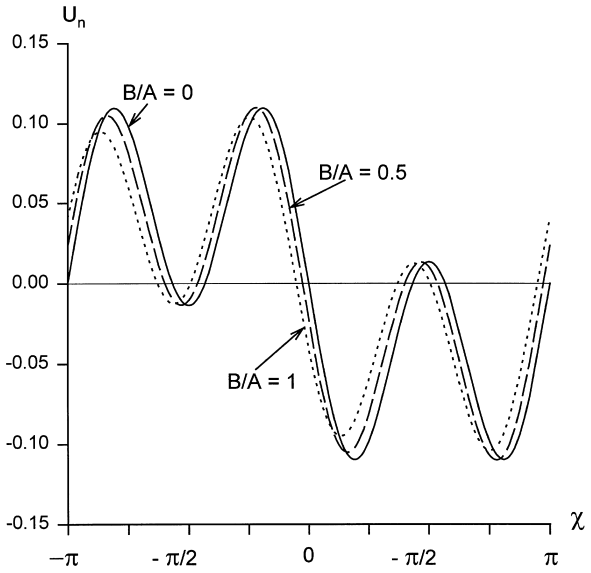

Fig. 5. Migration velocity normal to the fluid dividing streamline, as a function of cap orientation. Spherical caps with $\alpha = \pi/4$, $a = 0.5$. Cap orientation angle χ is angle (radians) between orientation vector **p** and x-axis. Shown for three cases of flow asymmetry: (a) $B/A = 0.0$ (symmetric flow); (b) $B/A = 0.5$ (high flow branch receives 72% of flow); (c) $B/A = 1.0$ (high flow branch receives 93% of flow) For each B/A, plot is for the point of intersection of the fluid dividing streamline and the line $x = -1$, $z = 0$. Other parameters R, h as in Fig. 1b.

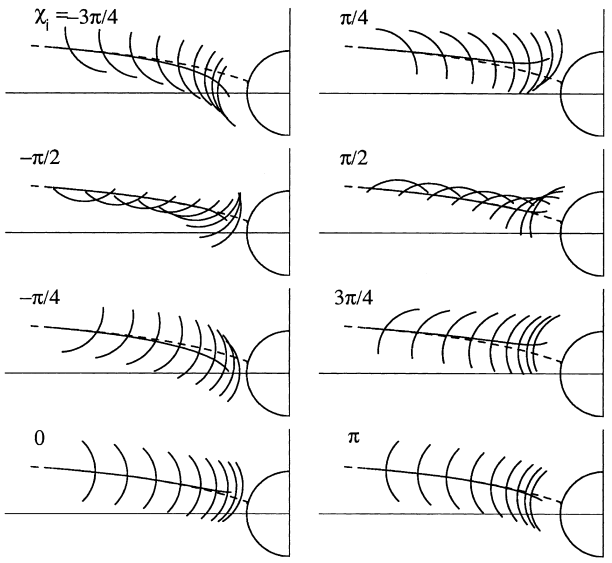

Fig. 6. Trajectories of spherical caps ($\alpha = \pi/4$, $a = 0.5$) with different initial orientations χ_i (angle between cap axis **p** and x-axis). Center of reaction is used as reference point. Dashed line shows fluid separating streamline. Parameters as in Fig. 1b.

streamline) at a point on the dividing streamline, as a function of particle orientation. This is for spherical caps placed in the flow of Fig. 1b. This is shown for several values of the ratio B/A that defines the asymmetry of the flow. The dividing streamline changes position as B/A changes; for each B/A, the plot is made for the point where this streamline intersects the plane $x = -1$. Migration is sensitive to orientation, but relatively insensitive to the asymmetry of the flow.

The sensitivity of migration to particle orientation is also seen in Fig. 6, which shows particle trajectories in the flow of Fig. 1b. The center of reaction is used as the reference point, and starts at the point $(-2.75, 0.536, 0)$, which lies on the fluid dividing streamline. As the particle approaches the dividing surface, it encounters a region of increasing extensional flow, with extension approximately in the y direction. As a result, the long axis of the particle tends to become aligned perpendicular with the flow, unless it is initially aligned with the flow. Fig. 7a shows the cap orientation χ_f at the instant that it passes the reference line indicated in Fig. 1b, as a function of its initial orientation χ_i. (This reference line is normal to the fluid dividing streamline at point B.) Orientation χ is defined as the angle from the x-axis to the cap orientation vector **p**, measured counterclockwise (the same convention used to define the angle θ in Fig. 1a). The final orientation is insensitive to the initial orientation for most angles, but highly sensitive for initial orientations near $\pm\pi/2$.

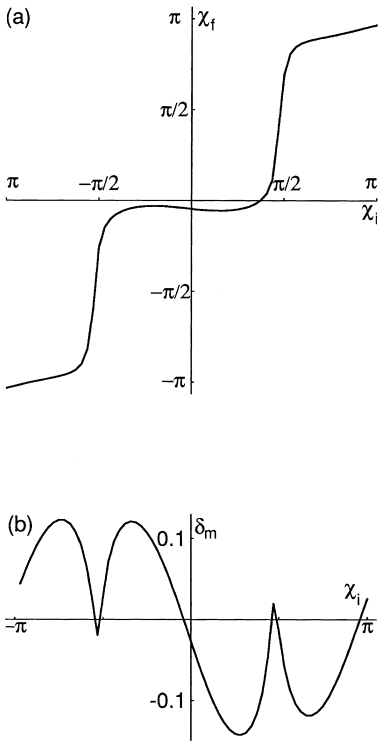

Fig. 7. (a) Cap orientation χ_f and (b) cap migration δ_m at reference line (C) (Fig. 1a) as functions of initial cap orientation χ_i. Parameter values as in Figs. 1b and 6.

The migration of particles as they cross the reference line is shown in Fig. 7b. Migration is measured as the distance between the point B (which lies on the fluid separating streamline), and the point of intersection of the center of reaction trajectory with the line C (Fig. 1b). Migration towards the high flow side (roughly in the $-y$ direction) is assigned a positive sign; in the opposite direction, it is negative. The variation of particle migration with initial orientation χ_i reflects the combined effects of the sensitive dependence of migration on particle orientation, shown in Fig. 6, and the flow-induced changes in particle orientation shown in Fig. 7a.

The migration shown in Fig. 7b is substantially larger than that expected for spheres of comparable size according to Faxen's Law. Therefore, the amount of particle migration in this flow is very dependent on particle shape and orientation. When averaged with respect to all possible initial orientations χ_i, the migration is close to zero. Multiple particles arriving with random, uniformly distributed orientations would therefore experience virtually no net migration. The actual distribution of orientations of red cells arriving at a bifurcation is, however, unlikely to be uniform, as a result of cell deformability and interactions, and cell alignment occurring at upstream bifurcations. Experimental observations suggest a tendency for red cells to assume shapes which are convex in front and concave in the rear. These effects cannot be estimated in the context of the present model, which assumes rigid cells.

4. Conclusions

The mechanics of red blood cell motion in bifurcations is complex, and all available models involve a number of simplifications. Here, the objective was to examine migration of particles approaching the dividing surface in a bifurcation whose downstream segments have similar diameters. Therefore, the interaction of the particles with the flow around the flow divider was emphasized by considering a geometry consisting of a cylindrical post between parallel plates. The motion of particles was predicted using a local linear or (for spheres) quadratic representation of the flow field. This approach neglects the effect of domain boundaries on the perturbation of the flow field by the particle, an approximation that becomes inaccurate when the particle closely approaches the dividing surface. A transverse straining flow is set up near the flow divider (Fig. 1b), and so relatively small migrations occurring more than one particle diameter upstream of the flow divider may have a significant effect on the particle's ultimate trajectory.

The main finding is that for spherical caps, particle migration is much larger than predicted for spheres of similar size in the same flow field, and depends in a complex way on initial particle orientation. The mean migration of a population of initially randomly oriented caps is nearly zero. Therefore, in order to estimate the contribution of particle migration to phase separation in bifurcations, information is required about the distributions of particle shapes and orientations upstream of the bifurcation. Under some conditions, the orientations of red blood cells can be stabilized, with "tank-treading" motion of the membrane around the cell interior (Goldsmith and Marlow, 1972, 1979). The resulting non-uniform distribution of orientations may lead to net shape-dependent migration across the separating streamsurface. The results shown in Fig. 5 suggest that the shape-dependent migration is relatively insensitive

to the asymmetry of the flow approaching the flow divider. However, in a vascular bifurcation, the position of the separating streamsurface depends on the division of flow between the branches. If the distribution of particle orientations varies within the cross-section of the parent vessel, the net migration may depend on the flow asymmetry.

In summary, these analyses suggest that the assumption made in previous models of bifurcations, that red cells follow fluid streamlines, is justified if cells approach the bifurcations with random orientations. However, actual distributions of red cell orientations in the parent vessel may be non-uniform, as a result of cell deformability and cell–cell interactions. Further progress in modeling the motion of red cells in diverging bifurcations is likely to depend on improved understanding of red cell motion in unbranched vessels.

Acknowledgements

This work was supported by NIH grants HL07249 and HL34555. Its contents are solely the responsibility of the authors and do not necessarily represent the official views of the National Institutes of Health.

Appendix A. Evaluation of coefficients in solution for base flow

According to Eqs. (5)–(7) and (17)–(19), the components of velocity are:

$$v_r = \left[-\frac{A_0'}{r^2}\cos\theta - \sum_{m=1}^{\infty}\frac{A_{0,\,m}}{r^{m+1}}\sin(m\theta)\right]\left(1-\frac{z^2}{h^2}\right) + Re\sum_{n=1}^{\infty}\left[\frac{1}{2\alpha_n}\left(A_n' + iB_n'\right)\left[K_2(\alpha_n r) + K_0(\alpha_n r)\right]\cos\theta + \sum_{m=1}^{\infty}\frac{1}{2\alpha_n}\left(A_{n,\,m} + iB_{n,\,m}\right)\left[K_{m+1}(\alpha_n r) + K_{m-1}(\alpha_n r)\right]\sin m\theta\right]\frac{\mathrm{d}q_n(z)}{\mathrm{d}z} - \sum_{n=0}^{\infty}\left[\frac{C_n'}{r}K_1(k_n r)\cos\theta - \sum_{m=1}^{\infty}\frac{1}{r}C_{n,\,m}K_m(k_n r)m\,\sin(m\theta)\right]\cos(k_n z); \tag{A1}$$

$$v_\theta = \left[-\frac{A_0'}{r^2}\sin\theta + \sum_{m=1}^{\infty}A_{0,\,m}\frac{1}{r^{m+1}}\cos(m\theta)\right]\left(1-\frac{z^2}{h^2}\right) + Re\sum_{n=1}^{\infty}\left[\frac{1}{\alpha_n^2 r}\left(A_n' + iB_n'\right)K_1(\alpha_n r)\sin\theta - \sum_{m=1}^{\infty}\frac{m}{\alpha_n^2 r}\left(A_{n,\,m} + iB_{n,\,m}\right)K_m(\alpha_n r)\cos m\theta\right]\frac{\mathrm{d}q_n(z)}{\mathrm{d}z} - \sum_{n=0}^{\infty}\left[C_n'\frac{k_n}{2}\left[K_2(k_n r) + K_0(k_n r)\right]\sin\theta + \sum_{m=0}^{\infty}C_{n,\,m}\frac{k_n}{2}\cos(m\theta)\left[K_{m+1}(k_n r) + K_{m-1}(k_n r)\right]\right]\cos(k_n z); \tag{A2}$$

$$v_z = Re\sum_{n=1}^{\infty}\left[\left(A'_n + iB'_n\right)K_1(\alpha_n r)\cos\theta + \sum_{m=0}^{\infty}\left(A_{n,\,m} + iB_{n,\,m}\right)K_m(\alpha_n r)\sin m\theta\right]q_n(z); \tag{A3}$$

where use has been made of the identity

$$\frac{\partial K_m(\alpha_n r)}{\partial r} = -\frac{\alpha_n}{2}\left[K_{m+1}(\alpha_n r) + K_{m-1}(\alpha_n r)\right]. \tag{A4}$$

We now impose the no-slip condition on the post. For the r and θ components, we expand in series analogous to Eqs. (12) and (13):

$$v_r|_{r=R} = \sum_{n=0}^{\infty}\left[E'_n\cos\theta + \sum_{m=1}^{\infty}E_{n,\,m}\sin m\theta\right]\cos k_n z; \tag{A5}$$

$$v_\theta|_{r=R} = \sum_{n=0}^{\infty}\left[F'_n\sin\theta + \sum_{m=0}^{\infty}F_{n,\,m}\cos m\theta\right]\cos k_n z. \tag{A6}$$

From the following expansions (Lee and Fung, 1969):

$$1 - \frac{z^2}{h^2} = \sum_{n=0}^{\infty}\frac{32(-1)^n}{\pi^3(2n+1)^3}\cos k_n z; \tag{A7}$$

$$\frac{\mathrm{d}q_n(z)}{\mathrm{d}z} = -\sum_{j=0}^{\infty}\frac{4(-1)^j k_j\alpha_n^2}{h^2\left(\alpha_n^2 - k_j^2\right)^2}\cos k_j z; \tag{A8}$$

it is found that

$$E'_n = -\frac{A'_0}{R^2}\frac{32(-1)^n}{\pi^3(2n+1)^3} - \frac{C'_n}{R}K_1(k_n R) - Re\sum_{j=1}^{\infty}\frac{1}{2\alpha_j}\left(A'_j + iB'_j\right)\left[K_2(\alpha_j R) + K_0(\alpha_j R)\right] \cdot\frac{4(-1)^n k_n\alpha_j^2}{h^2\left(\alpha_j^2 - k_n^2\right)^2}; \tag{A9}$$

$$E_{n,\,m} = -\frac{A_{0,\,m}}{R_{m+1}}\frac{32(-1)^n}{\pi^3(2n+1)^3} + \frac{mC_{n,\,m}}{R}K_m(k_n R) - Re\sum_{j=1}^{\infty}\frac{1}{2\alpha_j}\left(A_{j,\,m} + iB_{j,\,m}\right)\left[K_{m+1}(\alpha_j R) + K_{m-1}(\alpha_j R)\right]\frac{4(-1)^n k_n\alpha_j^2}{h^2\left(\alpha_j^2 - k_n^2\right)}; \tag{A10}$$

$$F'_n = -\frac{A'_0}{R^2}\frac{32(-1)^n}{\pi^3(2n+1)^3} - C'_n\frac{k_n}{2}\left[K_2(k_nR)+K_0(k_nR)\right] - Re\sum_{j=1}^{\infty}\frac{1}{\alpha_j^2 R}\left(A'_j + iB'_j\right) K_1(\alpha_j R)\frac{4(-1)^n k_n\alpha_j^2}{h^2\left(\alpha_j^2 - k_n^2\right)}; \tag{A11}$$

$$F_{n,m} = -(1-\delta_{m,0})\frac{A_{0,m}}{R^{m+1}}\frac{32(-1)^n}{\pi^3(2n+1)^3} + C_{n,m}\frac{k_n}{2}\left[K_{m+1}(k_nR)+K_{m-1}(k_nR)\right] + Re\sum_{j=1}^{\infty}\frac{m}{\alpha_j^2 R}\left(A_{j,m}+iB_{j,m}\right)K_m(\alpha_j R)\frac{4(-1)^n k_n\alpha_j^2}{h^2\left(\alpha_j^2-k_n^2\right)}. \tag{A12}$$

With these expansions, the no-slip conditions can be seen to give the following algebraic equations:

$$E'_n = -a_n; \quad E_{0,m} = -b_m; \quad E_{n,m} = 0 \qquad \text{for } n > 0; \tag{A13}$$

$$F'_n = -c_n; \quad F_{0,m} = -d_m; \quad F_{n,m} = 0 \qquad \text{for } n > 0. \tag{A14}$$

Next, we consider the z component. Following Lee and Fung (1969), we introduce the expansion:

$$v_z|_{r=R} = \sum_{n=1}^{\infty}\left[D'_n\cos\theta + \sum_{m=1}^{\infty}D_{n,m}\sin m\theta\right]Y_n(z), \tag{A15}$$

where

$$Y_n(z) \equiv \frac{1}{\sqrt{2}}\left[\frac{\sin\lambda_n z}{\sin\lambda_n h} - \frac{\sinh\lambda_n z}{\sinh\lambda_n h}\right], \tag{A16}$$

and λ_n satisfies $\tan\lambda_n h = \tanh\lambda_n h$. The following properties of $q_n(z)$ and $Y_n(z)$ are needed:

$$\int_{-h}^{h} Y_n(z)\,Y_m(z)\,\mathrm{d}z = h\delta_{n,m}, \tag{A17}$$

where $\delta_{n,m}$ is the Kronecker delta, and

$$\int_{-h}^{h} q_n(z)\,Y_m(z)\,\mathrm{d}z \equiv \beta_{n,\,m}$$

$$= \frac{2\sqrt{2}\lambda_m^2\alpha_n}{\lambda_m^4-\alpha_n^4}(\tan(\alpha_n h)+\cot(\alpha_n h)) - \frac{\sqrt{2}\left(\alpha_n^2+\lambda_m^2\right)}{h\left(\lambda_m^2-\alpha_n^2\right)^2} + \frac{\sqrt{2}\left(\alpha_n^2-\lambda_m^2\right)}{h\left(\lambda_m^2+\alpha_n^2\right)^2}$$

$$+ \frac{2\sqrt{2}\alpha_n\lambda_m\tan(\alpha_n h)}{h}\left[\frac{\cot(\lambda_m h)}{\left(\lambda_m^2-\alpha_n^2\right)^2} - \frac{\coth(\lambda_m h)}{\left(\lambda_m^2+\alpha_n^2\right)^2}\right]. \tag{A18}$$

From these properties, and the no-slip condition, it follows that

$$D_n' = \frac{1}{h}Re\sum_{j=1}^{\infty}\left[\left(A_j'+iB_j'\right)\beta_{j,\,n}K_1(\alpha_j r)\right] = 0; \tag{A19}$$

$$D_{n,\,m} = \frac{1}{h}Re\sum_{j=1}^{\infty}\left[\left(A_{j,\,m}+iB_{j,\,m}\right)\beta_{j,\,n}K_m(\alpha_j r)\right] = 0; \tag{A20}$$

for $n = 1, 2, 3, \ldots$ and $m = 1, 2, 3, \ldots$. Eqs. (A13), (A14), (A19) and (A20) for the coefficients appearing in the velocity were solved numerically, using a Mathematica program.

References

Amini, J.A., Fallahyan, F., 1997. Flow analysis of red blood cell through microvascular bifurcations. Biomedical Sciences Instrumentation 33, 567–572.

Audet, D.M., Olbricht, W.L., 1987. The motion of model cells at capillary bifurcations. Microvasc. Res 33, 377–396.

Barnard, A.C.L., Lopez, L., Hellums, J.D., 1968. Basic theory of blood flow in capillaries. Microvasc. Res 1, 23–34.

Bretherton, F.P., 1962. The motion of rigid particles in a shear flow at low Reynolds number. J. Fluid Mech 14, 284–304.

Bugliarello, G., Hsiao, G.C.C., 1964. Phase separation in suspensions flowing through bifurcations: a simplified hydrodynamic model. Science 143, 469–471.

Chien, S., Tvetenstrand, C.D., Farrell Epstein, M.A., Schmid-Schöbein, G.W., 1985. Model studies on distributions of blood cells at microvascular bifurcations. Am. J. Physiol 248, H568–H576.

Ditchfield, R., Olbricht, W.L., 1996. Effects of particle concentration on the partitioning of suspensions at small divergent bifurcations. J. Biomech. Eng 118, 287–294.

Dorrepaal, J.M., 1984. The resistance tensors for a spherical cap in Stokes flow. Q. Jl. Mech. Appl. Math 37, 355–371.

Enden, G., Popel, A., 1992. A numerical study of the shape of the surface separating flow into two branches in microvascular bifurcations. J. Biomech. Eng 114, 398–405.

Fenton, B.M., Carr, R.T., Cokelet, G.R., 1985. Nonuniform red cell distribution in 20–100 μm bifurcations. Microvasc. Res 29, 103–126.

Goldsmith, H.L., Karino, T., 1980. Physical and mathematical models of blood flow: experimental studies. In: Cokelet, G., Meiselman, H.J., Brooks, D.E. (Eds.), Erythrocyte Mechanics and Blood Flow. Alan R. Liss, New York, pp. 165–194.

Goldsmith, H.L., Marlow, J.C., 1972. Flow behavior of erythrocytes. Part I: Rotation and deformation in dilute suspensions. Proc. R. Soc. Lond B 182, 351–384.

Goldsmith, H.L., Marlow, J.C., 1979. Flow behavior of erythrocytes. Part II: Particle motions in concentrated suspensions of ghost cells. J. Colloid Interface Sci 71, 383–407.

Happel, J., Brenner, H., 1973. Low Reynolds Number Hydrodynamics. Noordhoff, Leyden, The Netherlands.

Hochmuth, R.M., Sutera, S.P., 1970. Spherical caps in low Reynolds-number tube flow. Chem. Eng. Sci 25, 593–604.

Kim, S., Karrila, S.J., 1991. Microhydrodynamics: Principles and Selected Applications. Butterworth–Heinemann, Boston.

Lee, J.S., Fung, Y.C., 1969. Stokes flow around a circular cylindrical post confined between two parallel plates. J. Fluid Mech 37, 657–670.

Nir, A., Weinberger, H.F., Acrivos, A., 1975. Variational inequalities for a body in a viscous shearing flow. J. Fluid Mech 68, 739–755.

Perkkiö, J., Keskinen, R., 1983. Hematocrit reduction in bifurcations due to plasma skimming. Bull. Math. Biol 45, 41–50.

Pries, A.R., Albrecht, K.H., Gaehtgens, P., 1981. Model studies on phase separation at a capillary orifice. Biorheology 18, 355–367.

Pries, A.R., Ley, K., Claassen, M., Gaehtgens, P., 1989. Red cell distribution at microvascular bifurcations. Microvasc. Res 38, 81–101.

Rong, F.W., Carr, R.T., 1990. Dye studies on flow through branching tubes. Microvasc. Res 39, 186–202.

Schmid-Schönbein, G.W., Skalak, R., Usami, S., Chien, S., 1980. Cell distribution in capillary networks. Microvasc. Res 29, 103–126.

Skalak, R., Branemark, P.-I., 1969. Deformation of red blood cells in capillaries. Science 164, 717–719.

Tsay, R.-Y., Weinbaum, S., 1991. Viscous flow in a channel with periodic cross-bridging fibers: exact solutions and Brinkman approximation. J. Fluid Mech 226, 125–148.

Wu, W.-Y., Weinbaum, S., Acrivos, A., 1992. Shear flow over a wall with suction and its application to particle screening. J. Fluid Mech 243, 489–518.

Yan, Z.-Y., Weinbaum, S., Acrivos, A., 1991. Fluid skimming and particle entrainment into a small circular pore. J. Fluid Mech 229, 1–27.